Journal of Marine Science and Technology

Volume 32 | Issue 2 Article 2

Numerical Study on the Aerodynamic Performance of Four Flettner Rotors by Varying Distance and Spin Ratio

Janghoon Seo
Shipbuilding & Marine Simulation Center, Tongmyong University, Busan, Republic of Korea

Dong-Woo Park
Department of Marine Mobility, Tongmyong University, Busan, Republic of Korea, dwpark@tu.ac.kr

Recommended Citation

Seo, Janghoon and Park, Dong-Woo (2024) "Numerical Study on the Aerodynamic Performance of Four Flettner Rotors by Varying Distance and Spin Ratio," *Journal of Marine Science and Technology*: Vol. 32: Iss. 2, Article 2.
DOI: 10.51400/2709-6998.2735
Available at: https://jmstt.ntou.edu.tw/journal/vol32/iss2/2

RESEARCH ARTICLE

Numerical Study on the Aerodynamic Performance of Four Flettner Rotors by Varying Distance and Spin Ratio

Janghoon Seo [a], Dong-Woo Park [b,*]

[a] Shipbuilding & Marine Simulation Center, Tongmyong University, Busan, Republic of Korea
[b] Department of Marine Mobility, Tongmyong University, Busan, Republic of Korea

Abstract

The Flettner rotor is a wind-assisted propulsion system applied in eco-friendly ship to reduce greenhouse gas emissions. As the requirements of international regulations on greenhouse gas emissions become increasingly strict, multiple Flettner rotors are being applied, necessitating the evaluation of their performance with varying design parameters. The present study focuses on the aerodynamic performances of four Flettner rotors with variable design parameters of distance and spin ratio. Distances and spin ratios, including relative spin ratios, are considered. The drag and lift coefficients and lift-to-drag ratio of Flettner rotors are determined using Computational Fluid Dynamics (CFD), and the associated flow fields are assessed. It is confirmed that the windward Flettner rotor shows better aerodynamic performance compared to the leeward Flettner rotor at constant spin ratio for all Flettner rotors. The aerodynamic performance of the leeward Flettner rotor proves to be sensitive to variations in distance and spin ratio, which are attributed to the deflected and unstable flows occurring downstream of the windward Flettner rotor. The effects of spin ratio and distance on total drag and lift coefficients and lift-to-drag ratio are also investigated. The findings of the present study have the potential to enhance the applicability in the design and operation of Flettner rotors. The additional assessment of the performance of Flettner rotors under different design parameters and number of Flettner rotors can be supplemented through future research.

Keywords: Multiple Flettner rotor, Magnus effect, Computational Fluid Dynamics

1. Introduction

Under the International Maritime Organization (IMO) regulations aimed at reducing greenhouse gas emissions by 50% by 2050, various approaches are being considered to decrease the vessel fuel consumption [1,2]. Recently, IMO regulations have been strengthened to require net-zero greenhouse gas emissions by 2050 [3,4]. One of the practical approaches for energy saving in commercial vessels is wind-assisted propulsion utilizing eco-friendly energy.

The representative wind-assisted propulsion is the Flettner rotor [5]. It generates assistant propulsion through the lift force produced by the Magnus effect [6], which is induced by a rotating cylinder located in the freestream. Flettner rotors are being practically applied on commercial ships, and to achieve greater assistant propulsion, multiple Flettner rotors are being employed. Researches on Flettner rotors have been conducted by various previous researchers which were mostly focused on the evaluation of the aerodynamic performance of a single Flettner rotor.

Received 12 November 2023; revised 9 March 2024; accepted 11 March 2024.
Available online 21 June 2024

* Corresponding author.
E-mail address: dwpark@tu.ac.kr (D.-W. Park).

https://doi.org/10.51400/2709-6998.2735

Badalamenti [7] conducted an experimental study to investigate the impact of cylinder endplates on the aerodynamic performance of a rotating cylinder placed in crossflow. While the endplates enhanced the lift and lift-to-drag ratio, they led to a limiting lift coefficient regardless of end conditions. Larger endplates delayed this plateau to higher velocity ratios, with the endplate size influencing drag behavior based on velocity ratio. Bordogna et al. [8] performed experiments of a large-scale Flettner rotor with high Reynolds numbers up to 1.0×10^6. They noted that the Reynolds number influences the lift coefficient primarily within the critical flow region and at velocity ratios below 2.5, whereas drag coefficients were sensitive to Reynolds number within the velocity ratio between 1 and 2.5.

Craft et al. [9] conducted Computational Fluid Dynamics (CFD) analysis to investigate the performance of the Flettner rotor. The result of CFD calculation showed close agreement with that of experiment and effect of Thom disk [10] was assessed. De Marco et al. [11] utilized CFD analysis to investigate the aerodynamic performance of the single Flettner rotor based on various design variables. The main design parameters of the spin ratio, aspect ratio, and endplate configurations were considered. As the aspect ratio and end plate size increased, the C_L/C_D value also increased. The significant reduction in hull resistance, up to approximately 30%, was achieved as a result of the design of the Flettner rotor. Kwon et al. [12] conducted CFD analysis for the performance of the Flettner rotor with several turbulence models and boundary conditions. The results of CFD analysis were compared with those of experiments and parametric studies with aspect ratio between 4 and 6 and diameter ratio between 1.5 and 8 were conducted.

In addition to the studies of single Flettner rotor, the interaction of multiple Flettner rotors was studied. Bordogna et al. [13] expanded their previous study [8] by an experimental investigation of the interaction effects on the aerodynamic performance of two Flettner rotors. The distance between two Flettner rotors was considered as 3, 7.5 and 15 diameters, and velocity ratios of 1, 1.5 and 2 were considered. The researchers highlighted that the aerodynamic performance of the two Flettner rotors is influenced by their interaction, particularly when they are positioned closer together and aligned with the wind direction. Moreover, the spin ratio substantially influenced the interaction on Flettner rotor. Chen et al. [14] experimentally investigated the aerodynamic performance of a large-scale Flettner rotors. The researchers categorized the initial, increasing, decreasing and stable areas to describe the variation in the lift-to-drag and velocity ratios for a single and two Flettner rotors.

Garzón and Figueroa [15] conducted experiment and numerical analysis of four Flettner rotors with single rotation of each Flettner rotor. They compared the results of experiments with numerical analysis. The results were limited to the one arrangement and single rotation of Flettner rotor. Kume et al. [16] compared the aerodynamic performances of four Flettner rotors between wind tunnel test and CFD analysis. The results of CFD simulation had the similar trend as those of model test. Effects of velocity ratio, wind direction, wind profile and interaction between Flettner rotors and superstructures on the ship were investigated. And they found lower drag force when velocity ratio is over 4.0 than that with velocity ratio under 2.0. In their study, the locations of four Flettner rotors were fixed and velocity ratios of Flettener rotors were identically applied. Lv et al. [17] investigated the aerodynamic performance of the Flettner rotors on the semi-submersible ship using CFD simulation. They investigated effects of spin ratio and wind direction to aerodynamic performance of Flettner rotors. The maximum lift coefficient was found at spin ratio of 3.0 and the maximum lift coefficients of two Flettner rotors were occurred when the apparent wind angle is 150°. Additionally, lift-to-drag ratio of windward Flettner rotor increased when distance between the two Flettner rotors decreases. In other words, lift-to-drag ratio of leeward Flettner rotor increases when distance between the two Flettner rotor increases. Tilling and Ringberg [18] developed the ShipCLEAN model, which predicts ship performance, to consider the performance of Flettner rotors using analytical and empirical methods. However, the performance and interaction effects of Flettner rotors were based on existing research results, and the effect of locations of Flettner rotors was not considered.

Recently, Flettner rotors are expected to be utilized with large size and increasing numbers to enhance the assistant propulsion [19]. Moreover, the number of Flettner rotors applied to the commercial ships is progressively increased [20]. Garzón and Figueroa [15] conducted experimental study for the four Flettner rotors. Particle Image Velocimetry was applied for the flow field around Flettner rotors with different rotational directions. Kume et al. [16] conducted experiments and numerical analysis on ship and Flettner rotors interactions, focusing on a fixed arrangement of four Flettner rotors and comparing experimental results with CFD simulations.

To our knowledge, previous researches focused on assessing the aerodynamic performance of a

single Flettner rotor or interactions between two Flettner rotors. Previous studies with multiple Flettner rotors were limited by a fixed rotational speed or arrangement.

Consequently, there is a necessity for the research on the wide range of design parameters of distance and rotational speed for many Flettner rotors in practical arrangement. Such research could significantly contribute to the design and operation of multiple Flettner rotors.

Thus, the present study aims to assess the impact of design parameters on the aerodynamic performance of four Flettner rotors, considering interactions resulting from variations in distance and rotational speeds of four Flettner rotors. CFD analysis is employed to assess the aerodynamic performance and flow field of Flettner rotors. Finally, aerodynamic performances by various configurations and rotational speeds involving four Flettner rotors are assessed.

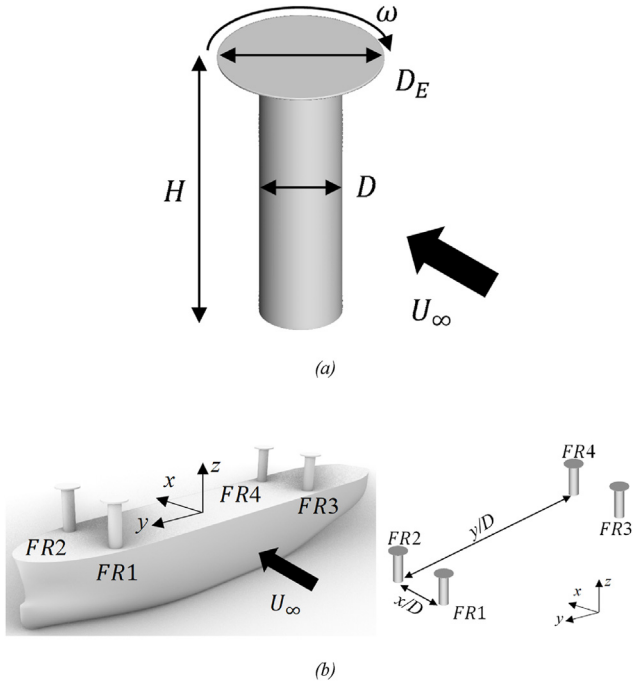

Fig. 1. Schematics of (a) definition of the Flettner rotor geometry and (b) arrangement and coordinate of Flettner rotors on the vessel.

2. Numerical setup

2.1. The Flettner rotors

In the present study, four Flettner rotors are considered. The dimensions of the Flettner rotors

Table 1. Parameters of Flettner rotor.

x/D		y/D		SR				
Case	Distance	Case	Distance	Case	FR1	FR2	FR3	FR4
XR1	6.5	YR1	25	SR01	1	1	1	1
XR2	5.5	YR2	20	SR02	2	2	2	2
XR3	4.5	YR3	15	SR03	3	3	3	3
		YR4	10	SR04	1	1	2	2
				SR05	2	2	3	3
				SR06	2	2	1	1
				SR07	3	3	2	2
				SR08	1	2	1	2
				SR09	2	3	2	3
				SR10	2	1	2	1
				SR11	3	2	3	2

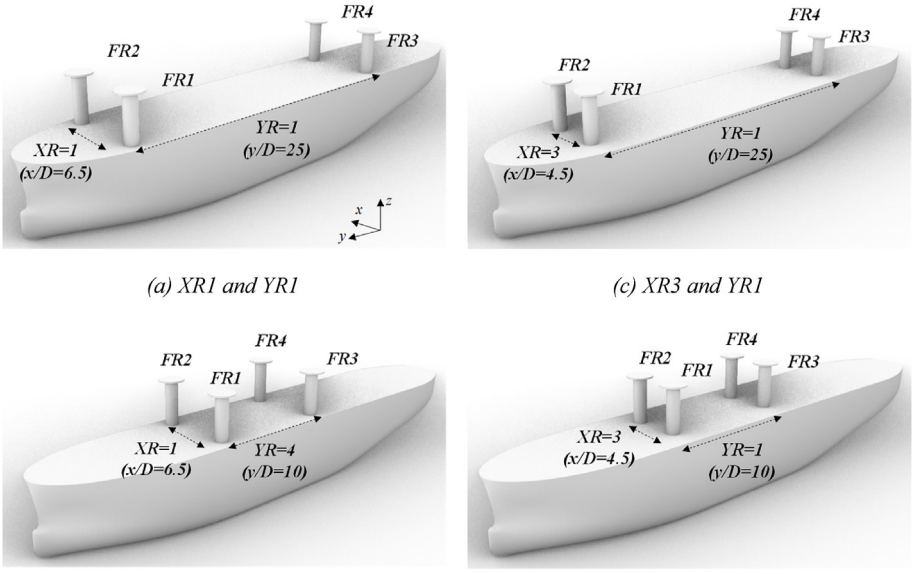

Fig. 2. Arrangement of Flettner rotors for maximum and minimum locations in the x and y directions.

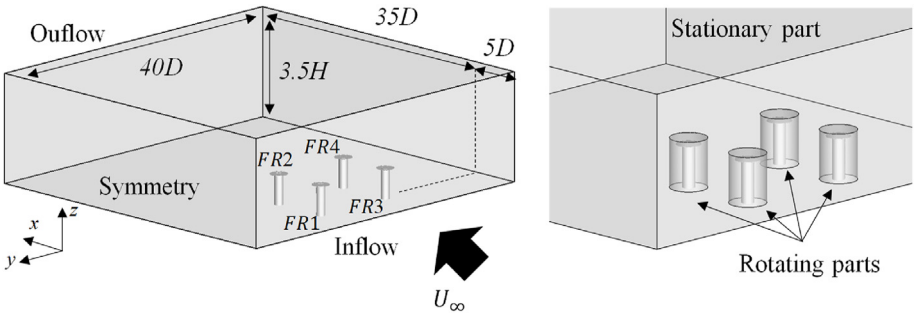

Fig. 3. Computational domain and boundary conditions.

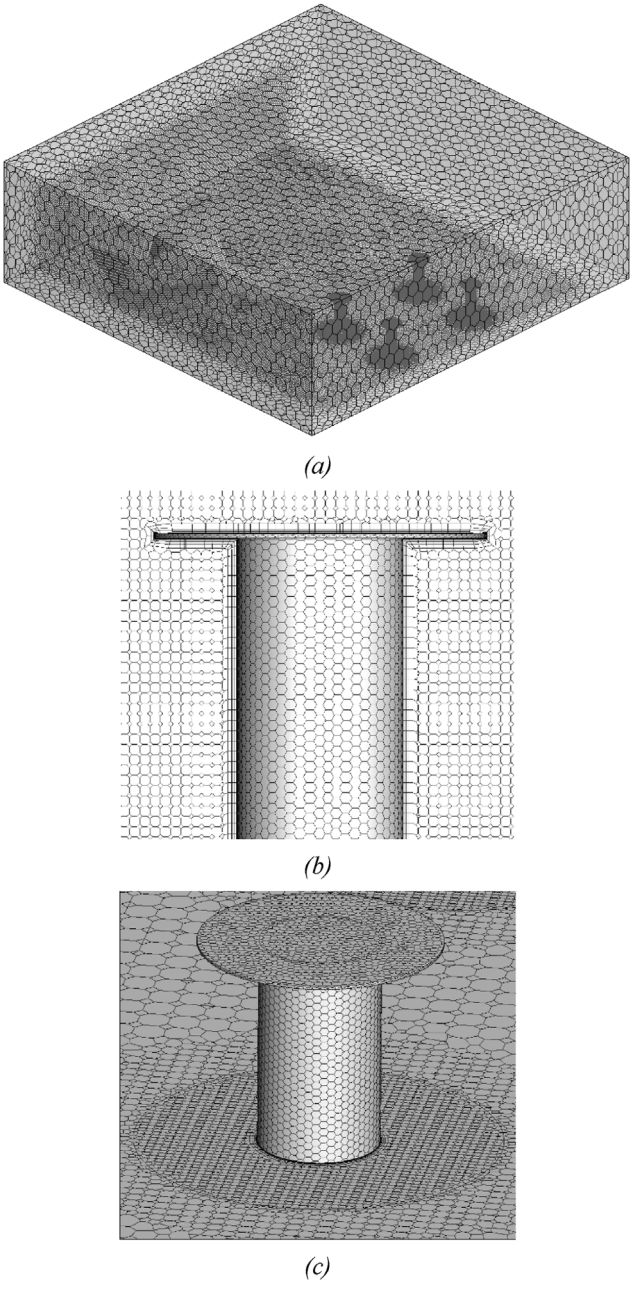

Fig. 4. Grid system: (a) perspective view, (b) surfaces of Flettner rotors and x-z plane and (c) surfaces of Flettner rotors and x-y plane.

are selected considering the main particulars and deck area of 50,000-ton oil tanker vessel which the Flettner rotors are to be installed, as shown in Fig. 1(a). The main dimensions of length, breadth and height of the vessel are 177, 32.2 and 23 m, respectively. The height (H) of the Flettner rotor is 14 m while the diameter (D) is 4 m. The diameter of Thom disk (D_E) attached to the top of the Flettner rotor is 1.5 times of the diameter for the Flettner rotor, resulting in a diameter of 6 m. Accordingly, the principal parameters of the Flettner rotor, the aspect ratio (H/D) and the diameter ratio (D_E/D) are set to 3.5 and 1.5, respectively.

The four Flettner rotors are arranged considering the deck area of the vessel, as shown in Fig. 1(b). Two Flettner rotors in the bow area are denoted as FR1 and FR2, while those in the stern area are denoted as FR3 and FR4. In order to assess the effect of positions on the Flettner rotors, distances in each direction are varied. Distances of 6.5, 5.5, and 4.5 in the freestream direction (x/D) and 25, 20, 15, and 10 in the transverse direction (y/D) are combined. The distances of x-direction for 6.5, 5.5 and 4.5 are defined as XR1, XR2 and XR3, respectively. In the same way, the distances of y-direction for 25, 20, 15 and 10 are defined as YR1, YR2, YR3 and YR4, respectively. The typical arrangements of Flettner rotors are presented in Fig. 2. Among the cases, the distances of XR1 and YR1 ($x/D = 6.5$ and $y/D = 25$) are the farthest combination among the cases as shown in Fig. 2(a). On the other hand, the distances of XR3 and YR4 ($x/D = 4.5$ and $y/D = 10$) have the closest arrangement among the cases as shown in Fig. 2(d). Cross-combinations of the longest and shortest distances for each direction are also presented in Fig. 2(b) and (c).

The wind direction is fixed from the port to the starboard sides which gives the highest thrust force by the lift force of Flettner rotor. The spin ratio (SR), which represents the ratio between wind speed and the rotational speed of the Flettner rotor, is considered as a variable parameter because it is the critical variable for the performance of Flettner rotor, as

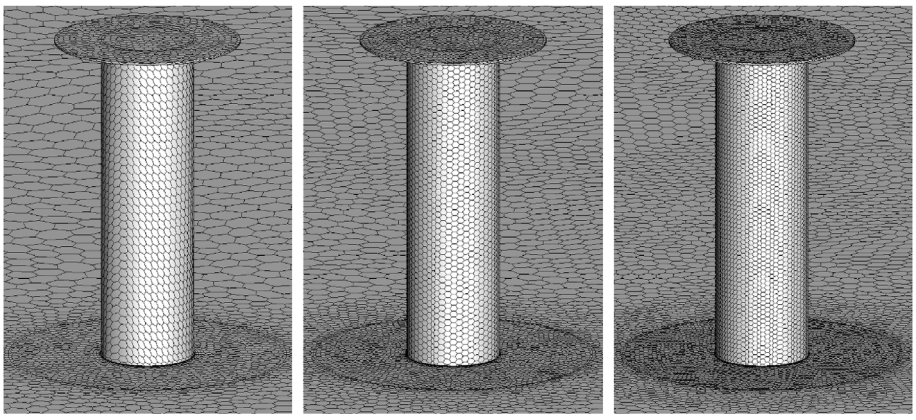

(a) (b) (c)

Fig. 5. Grid distributions of (a) Coarse, (b) Medium and (c) Fine models.

Table 2. Grid numbers and aerodynamic forces for the Flettner rotors.

Grid	Grid number	C_D				C_L			
		FR1	FR2	FR3	FR4	FR1	FR2	FR3	FR4
Coarse	1,000,000	1.647	3.779	1.665	3.842	6.212	5.761	6.192	5.676
Medium	2,500,000	1.647	3.852	1.664	3.902	6.306	5.834	6.283	5.735
Fine	5,000,000	1.641	3.902	1.678	3.943	6.311	5.834	6.304	5.726

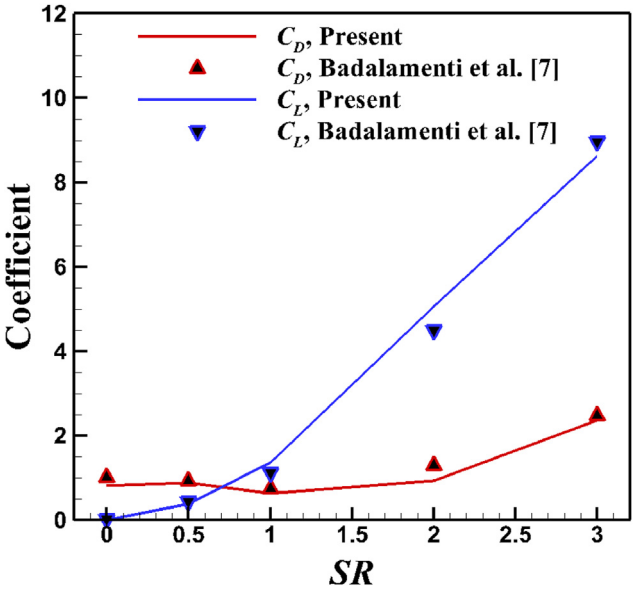

Fig. 6. Comparison of the present drag and lift coefficients with previous experimental result.

introduced in the previous studies [11–13,17]. In the present study, SR of 1.0, 2.0 and 3,0 are consistently considered for all Flettner rotors. Additionally, a relative difference of 1.0 to the spin ratio is applied between the bow and stern Flettner rotors and between the windward and leeward Flettner rotors to assess the effect of relative spin ratio. The spin ratios considered in the present study ranging from SR01 to SR11 are considered. In summary, a total of 132 cases with different positions and SRs, are employed in the present study, as summarized in Table 1.

2.2. Governing equations

The governing equations for unsteady incompressible viscous flow are the continuity and Navier–Stokes equations to solve the flow around the Flettner rotors. These equations can be presented in a Cartesian tensor form as:

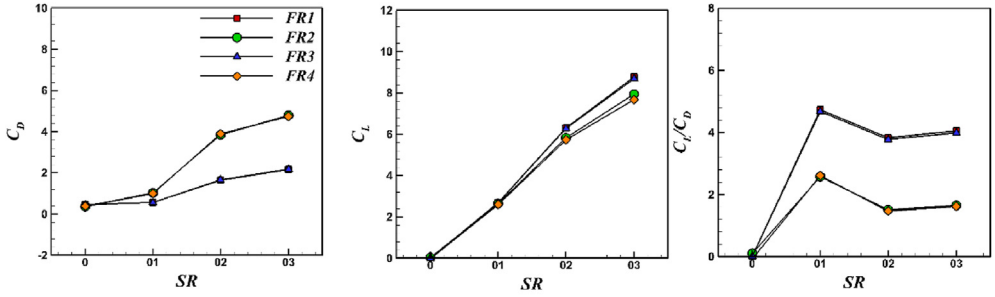

(a) (b) (c)

Fig. 7. Results of (a) drag coefficient, (b) lift coefficient and (c) lift-to-drag ratio of Flettner rotors according to SR at XR1 and YR1.

$$\frac{\partial u_i}{\partial x_i} = 0 \tag{1}$$

$$\frac{\partial}{\partial t}(\rho u_i) + \frac{\partial}{\partial x_i}(\rho u_i u_j) = -\frac{\partial P}{\partial x_i} + \frac{\partial}{\partial x_j}\left[\mu\left(\frac{\partial u_i}{\partial x_j} + \frac{\partial u_j}{\partial x_i}\right)\right] + \frac{\partial}{\partial x_j}\left(-\rho\overline{u_i' u_j'}\right) \tag{2}$$

where x_i is Cartesian coordinates, u_i is the corresponding velocity components, t is the time and p, ρ and μ are the pressure, density and viscosity, respectively.

The k-ω shear stress model (SST) turbulence model [21] which is successfully applied in the previous study [11,22] is applied to close the Reynolds stress term of $-\rho\overline{u_i' u_j'}$. For the rotation of Flettner rotors, the moving reference frame (MRF) scheme with interface boundary is employed. Further details of the information can be found in the Star CCM + manuals [23].

2.3. Computational domain boundary conditions

The present study adopts the moving reference frame technique which is achieved by directly rotating each subdomain including the Flettner rotor. Thus, the total computational domain is divided into stationary and four rotating parts, each defined by a cylinder surrounding the Flettner rotor, as presented in Fig. 3.

The outflow boundary is 35D away from the windward Flettner rotor. The farfield boundaries are 3.5H above the bottom and 40D along the y-direction. At the inlet boundary, a uniform velocity profile is imposed as the Dirichlet condition. The convective boundary condition, $-\partial u_i/\partial t + c\partial u_x/\partial x = 0$, is applied at the outlet boundary, where c is the space-averaged streamwise outlet velocity [24,25]. No-slip conditions are defined on the surfaces of Flettner rotors. Symmetry boundary condition is imposed on the farfield and bottom boundaries. Reynolds number based on free-stream velocity ($Re = U_\infty D/\upsilon$) is about 2.16×10^6 and time-step of 0.001 is applied. The simulation is conducted until fully developed steady or periodic force coefficients is achieved.

2.4. Grid system and validation

Figure 4 illustrates the polyhedral grid systems composed of stationary and rotating parts to realize the moving reference frame technique. The Cartesian cut-cell method is widely applied as a robust and efficient approach for generating high-quality grids for both simple and complex mesh generation problems [26]. The non-dimensional wall distance of y^+ is maintained close to 1, representing the distance of the first grid point. This specific value of y^+ is successfully applied in the previous researches [11,17]. To improve the accurate simulation of the Flettner rotors, a prismatic mesh layer is utilized

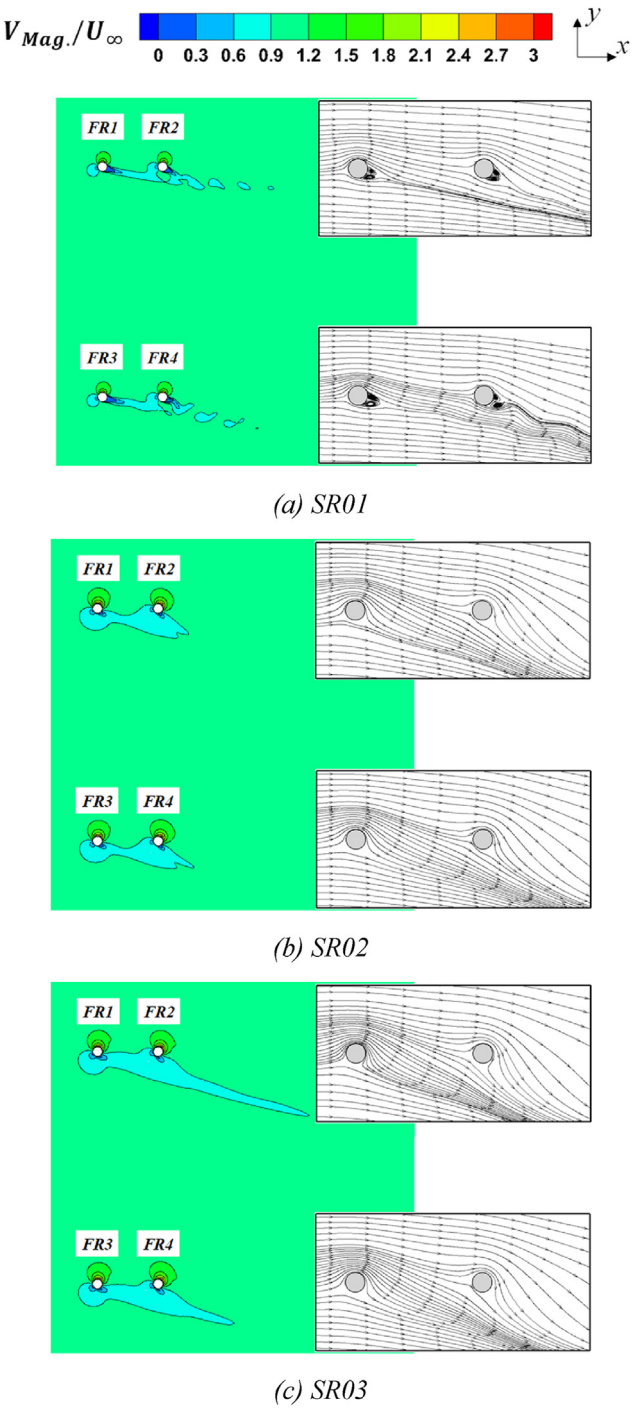

Fig. 8. Velocity vectors and contours of velocity magnitude in the horizontal plane (x-y) at z = 0.5H for XR1 and YR1.

near the wall of the Flettner rotor. This arrangement consists of fifteen prism layers with an expansion ratio of 1.5. The maximum grid spacing is approximately 1.0 m and is located near the outer boundary of the computational domain. The minimum grid spacing is approximately 0.0001 m near the Flettner rotor. The aspect ratio behind the Flettner rotor, excluding the prism layer region, is close to 1.0 across all directions.

The grid dependency test is conducted using three different grid configurations to assess the impact of grid systems on the time-averaged drag (C_D) and lift (C_L) coefficients which are defined as follows.

$$C_D = \frac{F_D}{\rho U_\infty{}^2 A} \tag{3}$$

$$C_L = \frac{F_L}{\rho U_\infty{}^2 A} \tag{4}$$

where F_D and F_L represent the time-averaged drag and lift forces, respectively, U_∞ denotes the free-stream velocity and A is the projected area of the Flettner rotor. The spin ratio of SR02 is selected as representative of the grid dependency test. Grid distributions of the coarse, medium and fine model close to Flettner rotor are presented in Fig. 5. Time-averaged aerodynamic coefficients for all test cases are compared with each other and the maximum differences of drag and lift coefficients among the test cases are 1.5% and 1.8%, respectively, as shown in Table 2. The results of the grid dependency test show that the differences of aerodynamic coefficients are not significant. Therefore, a medium grid system is employed for further study.

In order to validate numerical conditions, comparison of the performance of single Flettner rotor is carried out. Time-averaged drag and lift coefficients are employed for the validation. The analysis conditions and experimental results are obtained from

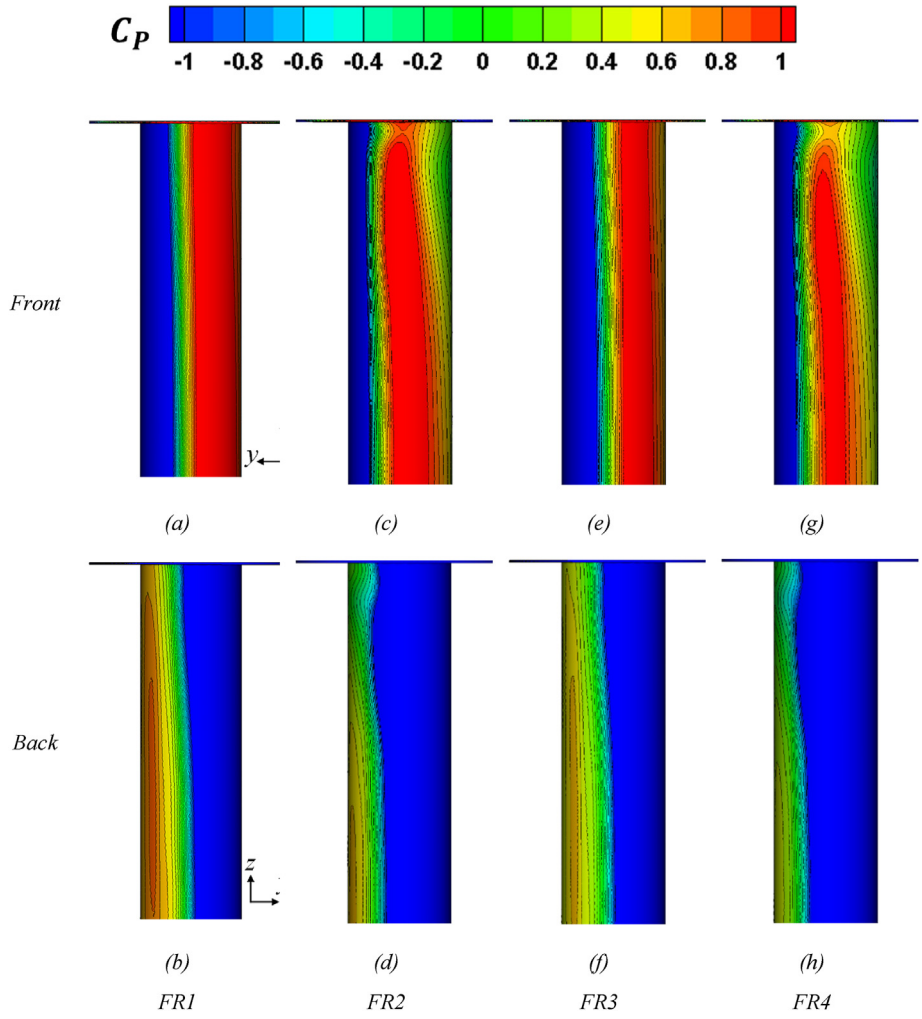

Fig. 9. Contours of pressure coefficients on surface of Flettner rotors for XR1 and YR1.

Balamenti et al. [7]. The present aerodynamic coefficients give good agreement with the experimental results over a range of spin ratios, as shown in Fig. 6. Therefore, the numerical approaches employed in the present study are suitable for evaluating the performances of Flettner rotors.

3. Results and discussion

3.1. Effect of spin ratio

The C_D, C_L and C_L/C_D of Flettner rotors at different spin ratios are compared in Fig. 7. To minimize the effect of the distance, the arrangement of Flettner rotors with XR1 and YR1 is representatively considered. In addition, the results of the stationary condition, where the Flettner rotor is not operating, are also included in Fig. 7.

When Flettner rotors are not rotating (SR = 0), C_L is negligible, resulting in a small C_L/C_D. As the spin ratio increases, the C_D and C_L are increased in all Flettner rotors as shown in Fig. 7(a) and (b), which is consistent with the previous results of single Flettner rotor [11,17]. For windward Flettner rotors of FR1 and FR3, they exhibit lower C_D and higher C_L values compared to leeward Flettner rotors of FR2 and FR4. The highest C_L/C_D appears at SR = 1 and decreased as SR increases for all Flettner rotors. The position of the Flettner rotor induces variations in aerodynamic force coefficients and lift-to-drag ratios. Windward Flettner rotors exhibit higher C_L/C_D than leeward Flettner rotors (Fig. 7(c)). Differences in C_D, C_L and C_L/C_D between FR1 and FR3 in bow area and between FR2 and FR4 in stern area are relatively small due to the decrease of interaction by larger distance between the Flettner rotors at the bow and stern.

In order to investigate the correlation between aerodynamic performance and the flow field, the comparisons of streamlines and contours of velocity magnitude around the Flettner rotors are performed in the horizontal plane at $z = 0.5H$, as shown in Fig. 8. The uniform free-stream flow is directed from left to right, while the rotation of Flettner rotor is clockwise when viewed from the top of the computational domain. In the case of SR = 1, an unstable flow distribution occurs in the downstream region due to the low rotational speed of the Flettner rotor. This characteristic of unstable flow is consistent with the finding of Seifert [27], implying that Von Karman vortices are formed when the spin ratio is less than 2. On the other hand, when SR increases to 2 and 3, the flow in the downstream region is stabled (Fig. 8(b) and (c)).

The flow behind Flettner rotors is deflected along the rotating direction. The flow deflection becomes stronger as the spin ratio increases. The deflected flow from windward Flettner rotor is extended to the upstream of leeward Flettner rotor. In addition, the low-speed velocity developed by the rotation of windward Flettner rotor is elongated to the upstream of FR2 and FR4. These explain differences in the drag and lift coefficients between windward (FR1 and FR3) and leeward (FR2 and FR4) Flettner rotors (Fig. 7).

At SR = 2, the distribution of pressure coefficient on the surface of the Flettner rotor is presented in Fig. 9. The surfaces observed from the inflow and

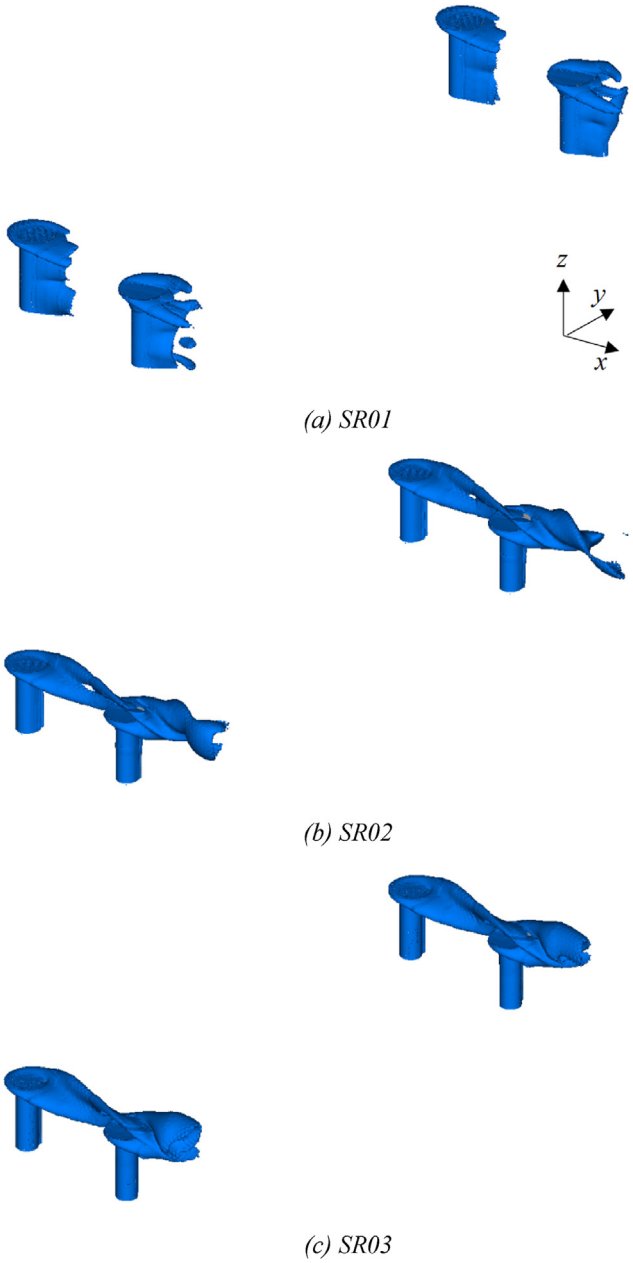

Fig. 10. Perspective view of the iso-surface of vorticity magnitudes for XR1 and YR1.

outflow boundaries are defined as “Front” and “Back”, respectively. High-pressure region on the surface of Flettner rotor is shifted owing to the deflected flow as explained in Fig. 8. The high-pressure regions of FR1 and FR3 are biased by the interaction between the freestream flow and the rotation of the Flettner rotor. However, in the case of FR2 and FR4, the high-pressure regions are positioned near the center of the Flettner rotor due to the deflected flow from the windward Flettner rotor.

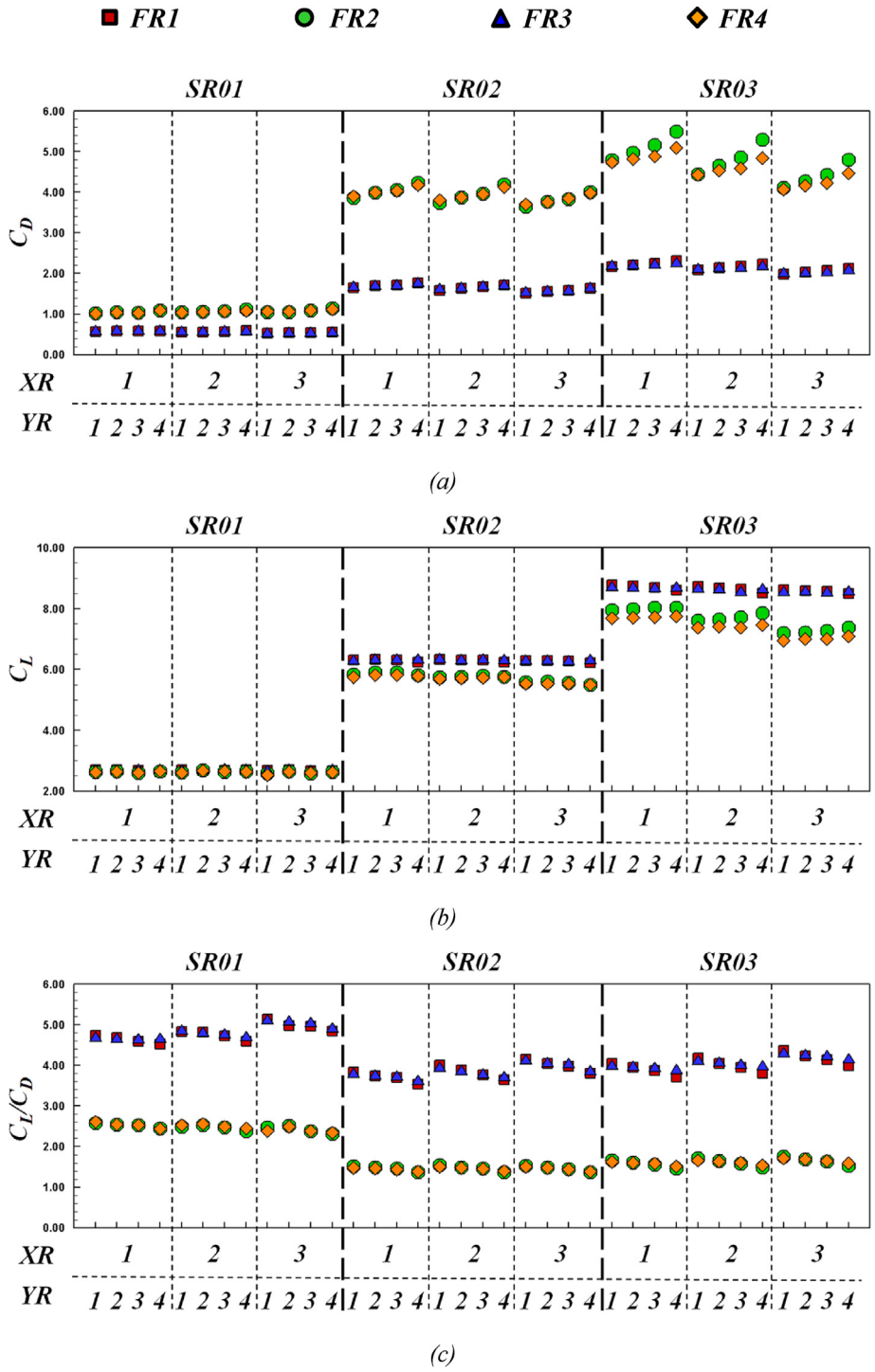

Fig. 11. Force coefficients according to relative distance of Individual Flettner rotors and spin ratios: (a) drag coefficients, (b) lift coefficients and (c) lift-to-drag ratio.

This difference of pressure distribution between windward and leeward Flettner rotor supports the differences of drag and lift coefficients.

In addition, non-uniform distribution of pressure along to height of Flettner rotor is exhibited due to the three-dimensional effect and interaction between the main rotor and Thom disc. This distribution is more clearly shown in the iso-surface of vorticity magnitude, as illustrated in Fig. 10. In cases of SR02 and SR03, leeward Flettner rotors are influenced by the three-dimensional flow downstream of windward Flettner rotors. Furthermore, as the spin ratio increases, it is evident that the three-dimensional vorticity becomes more dominant in the downstream flow, and the vorticity generated by the Thom disc becomes dominant compared with that generated by the main rotor.

3.2. Effect of distance among Flettner rotors

The distance between two rotating cylinders in tandem arrangement is another major parameter as

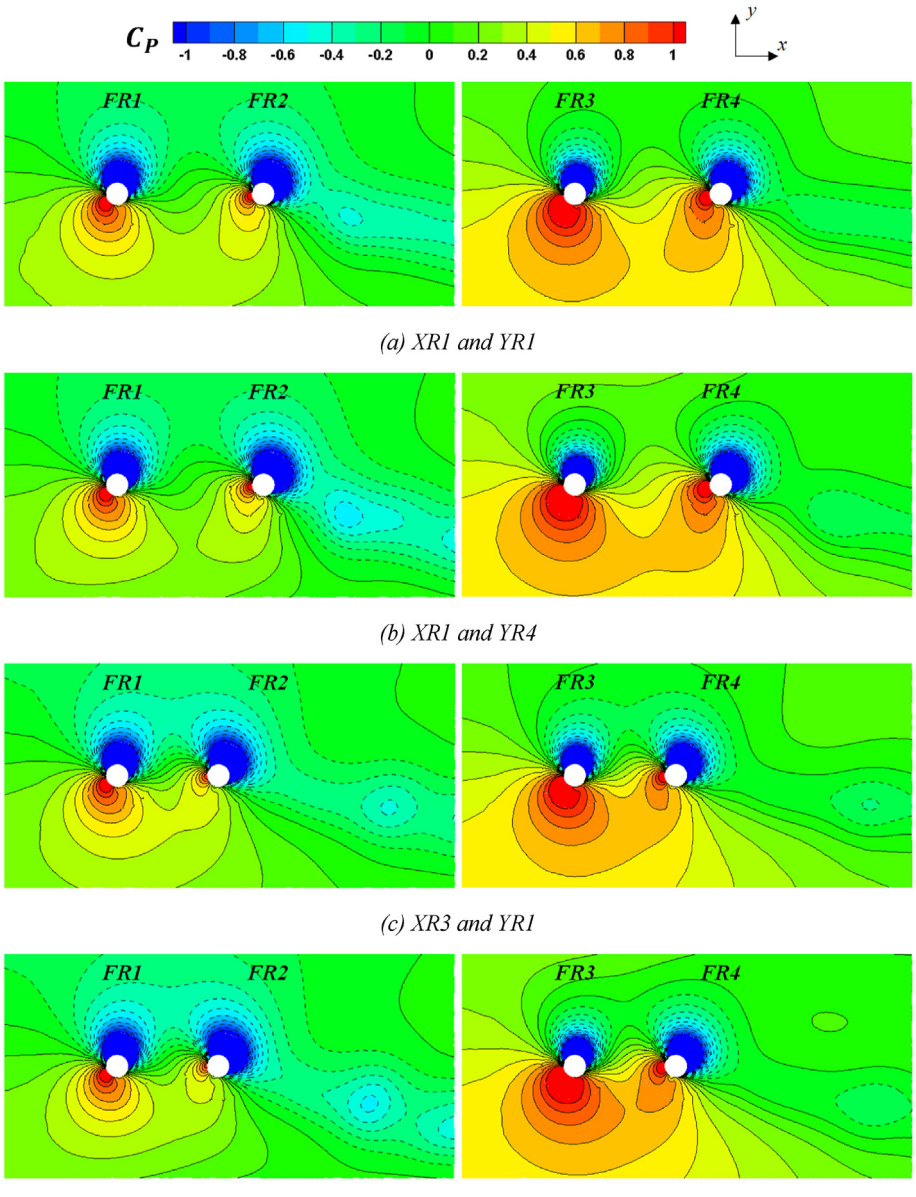

(a) XR1 and YR1

(b) XR1 and YR4

(c) XR3 and YR1

(d) XR3 and YR4

Fig. 12. Contours of pressure coefficients in the horizontal plane (x-y) at $z = 0.5H$.

confirmed in the previous researches [28–31]. To clarify the effect of distance, the aerodynamic force coefficients and lift-to-drag ratios for different distances are presented in Fig. 11. Spin ratios from SR01 to SR03 are considered.

The change in C_D and C_L for the windward Flettner rotor is relatively small. In contrast, effect of distance is relatively large for the leeward Flettner rotor. The effect of distance is especially outstanding as the spin ratio increases. This is because the upstream flow of the leeward Flettner rotor is changed by the windward Flettner rotor, while there are no interfering factors in the case of the windward Flettner rotor. In SR03, as XR decreases and YR increases, C_D increases for all cases. This difference in C_D decreases as spin ratio decreases. On the other hand, in SR03, the tendency of C_L is different for windward and leeward Flettner rotors. In the case of the windward Flettner rotor, C_L increases as XR and YR decrease. In the case of the leeward Flettner rotor, C_L increases as XR decreases and YR increases. In terms of lift-to-drag ratio, windward Flettner rotors have higher C_L/C_D than leeward Flettner rotors for all SRs. C_L/C_D increases as XR increases but decreases as YR increases. As a result, the maximum difference in C_L/C_D due to the variation in distance is about 13%, 17%, and 18% for the windward Flettner rotor in SR01, SR02, and SR03, respectively. The difference is about 11%, 12%, and 12% for the leeward Flettner rotor in SR01, SR02, and SR03, respectively.

Figure 12 shows the contours of pressure distributions in the horizontal plane at SR03. Distances of $x/D = 6.5$ and 4.5 and $y/D = 25$ and 10 which are the minimum and maximum distances for each direction are considered as representatives. The Flettner rotor rotates clockwise direction when viewed from the top, which implies rotating and freestream velocities are in the same direction on the upper side. This causes the increased speed, resulting in low pressure distribution on upper side. On the other hand, on the lower side, rotating and freestream velocities are in opposite directions. Due to the interaction of velocities on the lower side, the stagnation point of each Flettner rotor is located near the bottom, and high pressure is distributed.

When x/D decreases (Fig. 12(c) and (d)), windward and leeward Flettner rotors are closed each other, and low and high pressures are more correlated each other. Pressure distribution between the

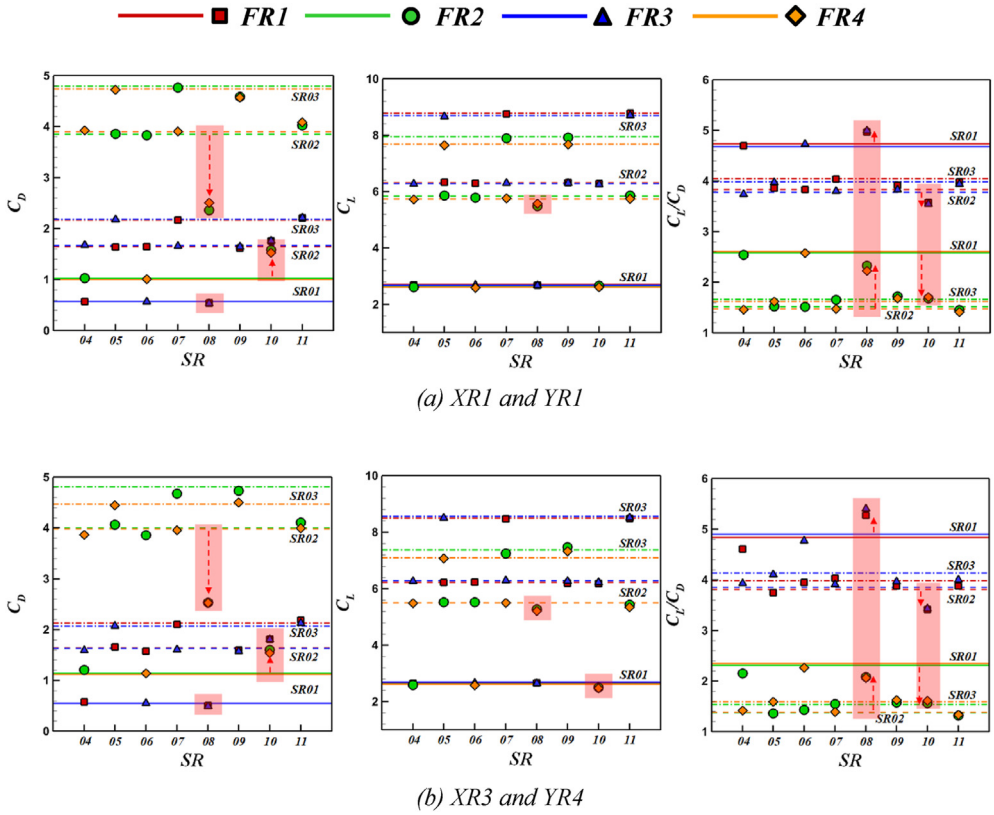

(a) XR1 and YR1

(b) XR3 and YR4

Fig. 13. Effect of variable spin ratios to drag coefficient (left column), lift coefficient (middle column) and lift-to-drag ratio (right column).

windward and leeward rotors changes rapidly. Due to changes of pressure distribution, flow deflection developed in the wake of windward Flettner rotor and high pressure area of the leeward Flettner rotor are reduced. This is consistent with the observed decrease of C_D and C_L values of FR2 and FR4 as x/D decreases. Pressure distribution on windward Flettner rotor is not significantly changed by the variation of x/D. In addition, the variation of y/D does not cause significant changes in the flow around Flettner rotors.

3.3. Effect of relative spin ratio

The differences in C_D, C_L and C_L/C_D are investigated in Fig. 13 for various relative spin ratios of each Flettner rotor. The horizontal lines represent Flettner rotors with identical spin ratios (SR01, SR02, and SR03). The coefficients for the cases ranging from SR04 to SR11, as defined in Table 1, are compared to assess the differences based on relative spin ratios. The distances of the Flettner rotors are considered for the farthest XR1 and YR1 cases

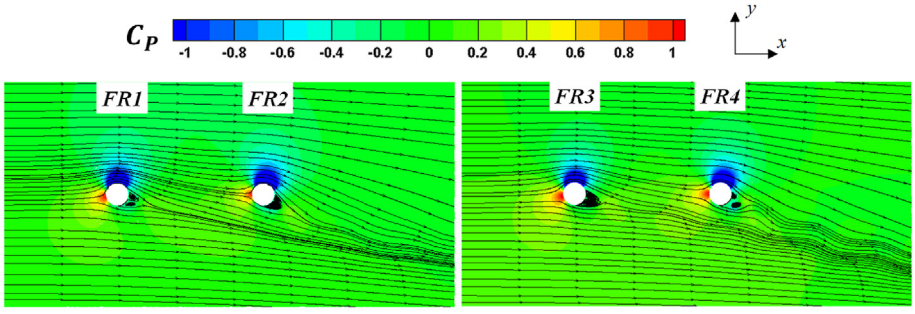

(a) SR01

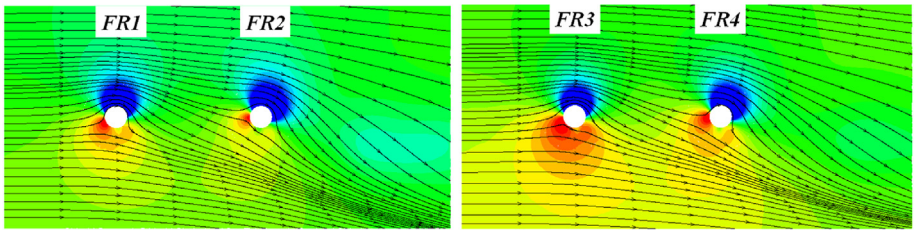

(b) SR02

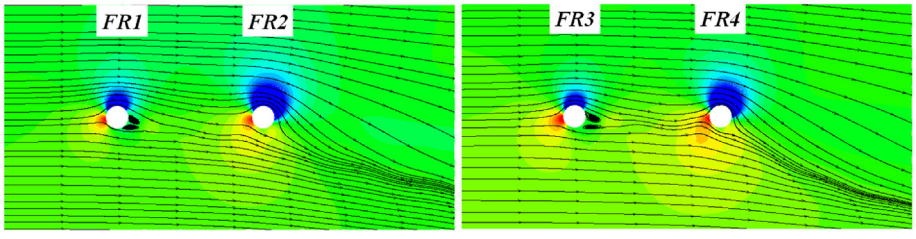

(c) SR08

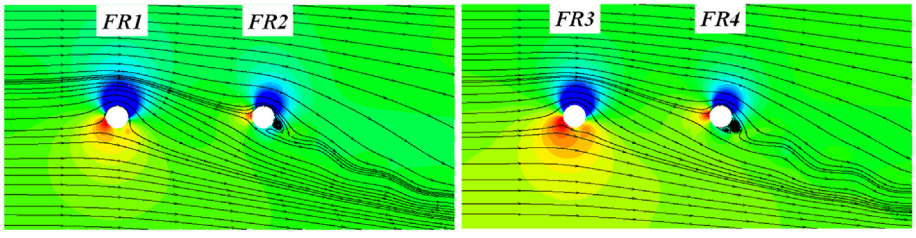

(d) SR10

Fig. 14. Contours of pressure coefficients and streamlines for XR1 and YR1 in the horizontal plane (x-y) at $z = 0.5H$.

(Fig. 13 (a)) and the closest XR3 and YR4 cases (Fig. 13(b)) in each direction.

From SR04 to SR07, the values of C_D, C_L and C_L/C_D are similar to those of SR01 and SR02. On the other hand, for SR08 to SR11, variations in spin ratios between the windward and leeward Flettner rotors results in an increased difference in the aerodynamic performance. For SR08 (SR = 1.0 for FR1 and FR3 and SR = 2.0 for FR2 and FR4) and SR10 (SR = 1.0 for FR2 and FR4 and SR = 2.0 for FR1 and FR3), differences of C_D, C_L and C_L/C_D are remarkable. In particular, reductions of C_D for FR2 and FR4 are significant in SR08, while those for FR1 and FR3 are relatively small. C_D values in SR10 are also increased, and FR2 and FR4 show clear increases. In the case of C_L, it is decreased in both SR08 and SR10 conditions, although this trend is not as substantial as observed in C_D. As a result of these changes in drag and lift coefficients, C_L/C_D s of all Flettner rotors are increased in SR08. In SR10, the C_L/C_D s of the all Flettner rotor are decreased. This tendency is reduced when the spin ratio increases, as observed in SR09 and SR11.

Figure 14 shows the distributions of pressure coefficient and streamlines at $z = 0.5H$, depending on the spin ratio. SR08 and SR10, which show the greatest changes in C_D, C_L and C_L/C_D in Fig. 13, and SR01 and SR02, which are employed as base horizontal lines, are selected. In the case of SR = 1, as shown in Fig. 8, unstable flow in downstream causes a small wake behind the Flettner rotor. In the case of SR02, the streamline becomes stable and the wake disappears. In the case of SR08, the spin ratios of the windward Flettner rotors are 1 and the development of a small wake is observed, similar as SR01. This also has an effect on the downstream of the leeward Flettner rotors, which have a spin ratio of 2. Similarly, in the SR10 condition, an unstable flow is developed in downstream of the leeward Flettner rotors with SR = 1. This supports the changes in C_D, C_L and C_L/C_D discussed in Fig. 13.

3.4. Total aerodynamic performance

The total C_D, C_L and C_L/C_D for the four Flettner rotors are shown in Fig. 15. Overall, C_D exhibits the same trend with changes in XR and YR as shown in Fig. 14(a). On the other hand, for C_L, the effects of XR and YR are not significant. In conclusion, C_L/C_D is distributed in accordance with the opposite tendency of the C_D (Fig. 15(c)). The case with the highest C_D and C_L is SR03, while the C_L/C_D is the highest in SR10, which is similar to SR01.

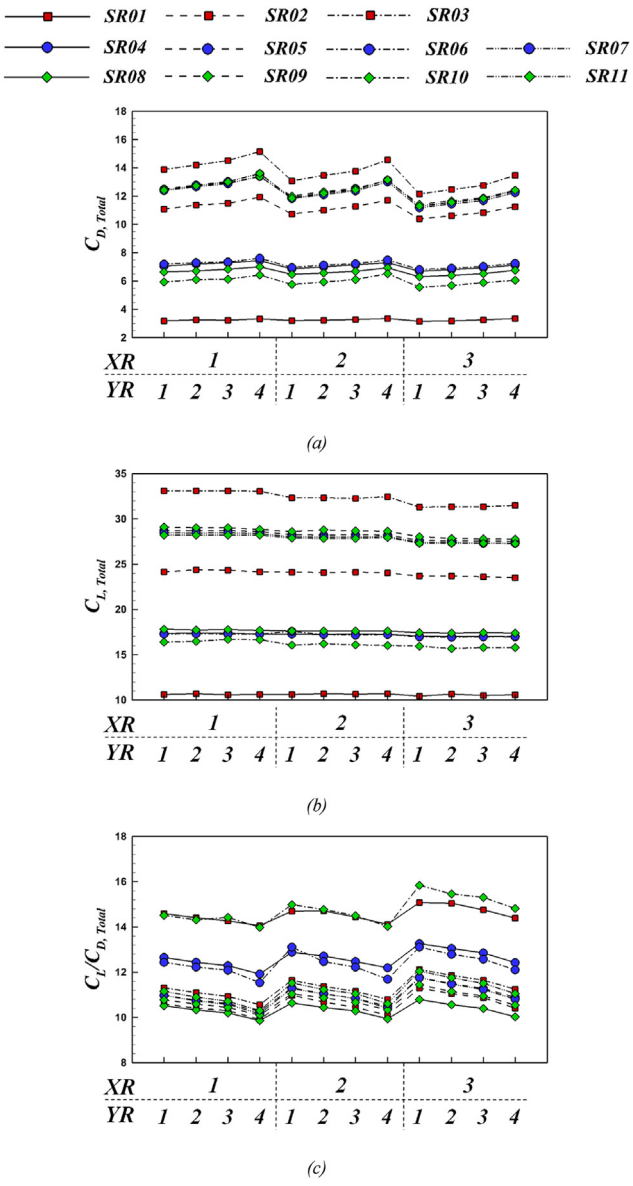

Fig. 15. Total force coefficients according to relative distance of Flettner rotors and spin ratios: (a) drag coefficients, (b) lift coefficients and (c) lift-to-drag ratio.

4. Conclusions

The present study numerically investigates the impact of design parameters, specifically the distance and spin ratio of Flettner rotors, on the aerodynamic performances of four Flettner rotors installed in oil tanker vessel using CFD analysis. The three distances in the freestream direction and the four distances in the transverse direction are taken into consideration. In addition, 12 different spin ratios, with relative spin ratio for each Flettner rotor are combined with the variations in distance.

The main results can be summarized as follows

- Impact of spin ratio: both drag and lift coefficients increase with higher spin ratios. Windward Flettner rotors exhibit lower drag and higher lift coefficients compared to leeward Flettner rotors. The differences in drag and lift coefficients between the bow and stern Flettner rotors are not significant.
- The effect of distances among Flettner rotors: The drag coefficients for leeward Flettner rotors are most impacted. This is because the deflected flow and low-velocity region that are developed at the downstream of the windward Flettner rotors extend to the leeward Flettner rotors. The maximum differences of lift-to-drag ratio by the effect of distance for windward and leeward Flettner rotors are about 18% and 12%, respectively.
- Impact of relative spin ratio: The greatest effect of the relative spin ratio occurs when the spin ratio between the windward and leeward rotors is small and different. These results disappear when the spin ratio increases. The relative spin ratio between the bow and stern is negligible.
- Total aerodynamic force coefficients: These reach their maximum when the spin ratio is large, and the Flettner rotors have the same spin ratio. The lift-to-drag ratio is maximized for the smallest spin ratio.

The present study considers various distances and spin ratios of Flettner rotors, and presents the aerodynamic performances and flow fields. The results of present study may contribute to the potential applicability in the design and operation of Flettner rotors. Therefore, the additional assessment of the performance of Flettner rotors with other design parameters and number of Flettner rotors can be supplemented through future research.

Conflicts of interest

There is no conflict of interest.

Acknowledgements

This work is supported by the Prototype-Virtual Integrated Technology Support for Basic Design of Mid-size Ships and Offshore Structures grant funded by the Korea government (MOTIE) through P0021213.

References

[1] Rutherford D, Comer B. The International Maritime Organization's initial greenhouse gas strategy. 2018.
[2] Halff A, Younes L, Boersma T. The likely implications of the new IMO standards on the shipping industry. Energy Pol 2019;126:277−86.
[3] Bullock S, Mason J, Larkin A. The urgent case for stronger climate targets for international shipping. Clim Pol 2022; 22(3):301−9.
[4] Lu B, Ming X, Lu H, Chen D, Duan H. Challenges of decarbonizing global maritime container shipping toward net-zero emissions. npj Ocean Sustain 2023;2(1):11.
[5] Flettner A. The flettner rotorship. Eng 1925;19:117−20.
[6] Swanson WM. The Magnus effect: a summary of investigations to date. 1961.
[7] Badalamenti C, Prince S. Effects of endplates on a rotating cylinder in crossflow. In: 26th AIAA applied aerodynamics conference. vol. 7063; 2008.
[8] Bordogna G, Muggiasca S, Giappino S, Belloli M, Keuning JA, Huijsmans RHM, et al. Experiments on a Flettner rotor at critical and supercritical Reynolds numbers. J Wind Eng Ind Aerod 2019;188:19−29.
[9] Craft TJ, Iacovides H, Johnson N, Launder BE. Back to the future: flettner-Thom rotors for maritime propulsion?. In: THMT-12. Proceedings of the seventh international symposium on turbulence heat and mass transfer. Begel House Inc.; 2012.
[10] Thom A. Effects of discs on the air forces on a rotating cylinder. Aero Res Counc R&M 1934;1623.
[11] De Marco A, Mancini S, Pensa C, Calise G, De Luca F. Flettner rotor concept for marine applications: a systematic study. Int J Rotating Mach 2016:3458750.
[12] Kwon CS, Yeon SM, Kim YC, Kim YG, Kim YH, Kang HJ. A parametric study for a flettner rotor in standalone condition using CFD. Int J Nav Archit Ocean Eng 2022;14: 100493.
[13] Bordogna G, Muggiasca S, Giappino S, Belloli M, Keuning JA, Huijsmans RHM. The effects of the aerodynamic interaction on the performance of two Flettner rotors. J Wind Eng Ind Aerod 2020;196:104024.
[14] Chen W, Wang H, Liu X. Experimental investigation of the aerodynamic performance of Flettner rotors for marine applications. Ocean Eng 2023;281:115006.
[15] Garzón F, Figueroa A. The study on the flow generated by an array of four Flettner rotors: theory and experiment. Appl Math 2017;8(12):1851−8.
[16] Kume K, Hamada T, Kobayashi H, Yamanaka S. Evaluation of aerodynamic characteristics of a ship with flettner rotors by wind tunnel tests and RANS-based CFD. Ocean Eng 2022; 254:111345.
[17] Lv J, Lin Y, Zhang R, Li B, Yang H. Assisted propulsion device of a semi-submersible ship based on the Magnus effect. Pol Marit Res 2022;29(3):33−46.
[18] Tillig F, Ringsberg JW. Design, operation and analysis of wind-assisted cargo ships. Ocean Eng 2020;211:107603.
[19] Wang Y, Zhang X, Lin S, Qiang Z, Hao J, Qiu Y. Analysis on the development of wind-assisted ship propulsion Technology and contribution to emission reduction. In: IOP conference series: earth and environmental science. 966. IOP Publishing; 2022. p. 012012 (1).
[20] Petković M, Zubčić M, Krčum M, Pavić I. Wind assisted ship PropulsionTechnologies−can they help in emissions reduction? NAŠE MORE: znanstveni časopis za more i pomorstvo 2021;68(2):102−9.
[21] Menter FR. Zonal two equation K-u turbulence models for aerodynamic flows. AIAA Paper 1993:93−2906.
[22] Garenaux M, Schot J, Eggers R. Numerical analysis of flattener rotors performances on the MARIN hybrid transition coaster. In: High-Performance Marine Vehicles (HIPER), Cortana, Italy; 2020. p. 297−313.
[23] CD-Adapco. Star-CCM+ user guide. 2021.
[24] Breuer M. Large eddy simulation of the subcritical flow past a circular cylinder: numerical and modeling aspects. Int J Numer Methods Fluid 1998;28:1281−302.

[25] Sohankar A, Davidson L, Norberg C. Large eddy simulation of flow past a square cylinder: comparison of different sub-grid scale models. J Fluid Eng 2000;122:39−47.
[26] Meinke M, Schneiders L, Gunther C, Schröder W. A cut-cell method for sharp moving boundaries in Cartesian grids. Comput Fluids 2013;85:135−42.
[27] Seifert J. A review of the Magnus effect in aeronautics. Prog Aero Sci 2012;55:17−45.
[28] Nemati H, Farhadi M, Sedighi K, Pirouz MM, Abatari NN. Convective heat transfer from two rotating circular cylinders in tandem arrangement by using lattice Boltzmann method. Appl Math Mech 2012;33:427−44.
[29] Darvishyadegari M, Hassanzadeh R. Convective heat transfer and fluid flow of two counter-rotating cylinders in tandem arrangement. Acta Mech 2018;229(4): 1783−802.
[30] Darvishyadegari M, Hassanzadeh R. Heat and fluid flow around two co-rotating cylinders in tandem arrangement. Int J Therm Sci 2019;135:206−20.
[31] Rastan MR, Sohankar A, Alam MM. Flow and heat transfer across two inline rotating cylinders: effects of blockage, gap spacing, Reynolds number, and rotation direction. Int J Heat Mass Tran 2021;174:121324.